

# D-Wave Superconductors near Surfaces and Interfaces: A Scattering Matrix Approach within the Quasiclassical Technique

T. Lück and U. Eckern

*Institut für Physik, Universität Augsburg, D-86135 Augsburg, Germany*

A. Shelankov

*Department of Theoretical Physics, Umeå University, 901 87, Sweden*

*A.F. Ioffe Physico-Technical Institute, 19021 St. Petersburg, Russia*

(November 21, 2018)

## Abstract

A recently developed method [A. Shelankov and M. Ozana, Phys. Rev. B **61**, 7077 (2000)] is applied to investigate  $d$ -wave superconductors in the vicinity of (rough) surfaces. While this method allows the incorporation of arbitrary interfaces into the quasiclassical technique, we discuss, as examples, diffusive surfaces and boundaries with small tilted mirrors (facets). The properties of the surface enter via the scattering matrix in the boundary condition for the quasiclassical Green's function. The diffusive surface is described by an ensemble of random scattering matrices. We find that the fluctuations of the density of states around the average are small; the zero bias conductance peak broadens with increasing disorder. The faceted surface is described in the model where the scattering matrix couples  $m$  in- and  $m$  out-trajectories ( $m \geq 2$ ). No zero bias conductance peak is found for [100] surfaces; the relation to the model of Fogelström *et al.* [Phys. Rev. Lett. **79**, 281 (1997)] is discussed.

## I. INTRODUCTION

The  $d_{x^2-y^2}$  symmetry of the order parameter (OP) in high temperature (high- $T_c$ ) superconductors is nowadays well established by various phase-sensitive experiments, the most striking being the observation of a half flux quantum in a tricrystal geometry by Tsui *et al.* [1]. Also the zero-bias conductance peak (ZBCP) found in different tunnel experiments [2–6] on [110]-oriented boundaries of  $\text{YBa}_2\text{Cu}_3\text{O}_{7-\delta}$  gave a strong hint for  $d$ -wave symmetry as was first pointed out by Hu [7]. However, in more recent experiments, several puzzling questions arose. For example a splitting of the ZBCP was observed [8] and ZBCP's were reported even for [100]-oriented junctions [8,9]. Disorder effects were examined as well in experiment where the disorder of the junctions was increased by ion irradiation [10]. A decreasing height of the ZBCP was observed whereas the width stayed constant.

The most successful approach to treat such inhomogeneous problems is the theory of quasiclassical Green's functions [11–13]. The properties of surfaces or interfaces are included by effective boundary condition. For a specular surface the Green's function has to be continuous on a classical trajectory (see Fig. 1). In this most simple model the pair-breaking effect of surfaces as well as the existence of a ZBCP can be explained: If quasiparticles are scattered to branches with a different OP ( $\alpha \neq 0$ ) the pairing is suppressed and bound states can occur due to Andreev scattering. If a quasiparticle is scattered with a sign change of the OP the ZBCP exists, too. In this framework it was also shown [14,15] that the splitting of the ZBCP is in agreement with the existence of a subdominant order parameter ( $d_{x^2-y^2} + id_{xy}/s$ ) in the vicinity of the surface. The generalization of the boundary conditions to a specular interface was carried out by Zaitsev [16]. In this situation the Green's function on four trajectories must match at the interface, which leads to quite complicated non-linear boundary conditions.

As surface roughness is present in experiments, models were developed to include disorder in the theory. One possibility, first suggested by Ovchinnikov [17], is to use the boundary conditions for the specular situation and cover the surface with a thin dirty layer where equations for the dirty case must be applied. In numerical studies of boundary problems similar techniques were used [18,19]. Also a scattering matrix approach, which is related to the randomly rippled wall model [21], was applied to disordered surfaces [22]; the solution was given in a Born-like approximation. Except for models with unitary scatterers [20], all calculations show a broadening of the ZBCP due to disorder.

Often the surface roughness is only present on scales much smaller than the coherence length. In this case, the boundary conditions for the quasiclassical Green's function can be formulated in terms of the scattering matrix ( $S$ -matrix), as it has been recently suggested in [24]. A rough interface does not conserve the momentum parallel to the surface, and, therefore, it couples waves (*i.e.* quasiclassical trajectories) with different propagation direction. The microscopic structure of the interface enters the theory via the  $S$ -matrix. In the absence of detailed knowledge about the microscopic structure of the surface, the  $S$ -matrix has to be taken as a phenomenological input.

Due to the very short in-plane coherence length in high- $T_c$  superconductors ( $\xi_0 \approx 20\text{\AA}$ ) structures on larger scales occur as well. Then the translational invariance parallel to the surface is lost on this length scale and a full 2D treatment of the problem is necessary, in which the trajectories are considered individually (see Fig. 2). For example, in cuprates

facets with typical dimensions of 10 – 100nm are present at interfaces [23]. This leads to the existence of a ZBCP even for [100] tunnel junctions as was pointed out by Fogelström *et al.* [15].

In our study we use the scattering matrix approach presented in [24] to describe surfaces with microscopic roughness. We will discuss two kinds of surfaces: First, we study a microscopically disordered surface, which is described by random matrices. In contrast to earlier calculations we are able to consider individual realizations of the disorder; we examine averaged quantities as well as fluctuations. Afterwards we focus on an  $S$ -matrix that describes a surface with tilted mirrors, where few trajectories are connected at the surface.

In the following section we will briefly introduce the quasiclassical theory for superconductors. Subsequently we will present the boundary conditions in the form most suitable for our purpose and discuss the general properties. In section III we derive the  $S$ -matrices for different situations and present the related results. We conclude with a discussion of our results and compare them to other approaches.

## II. METHOD

### A. Theory of quasiclassical Green's functions

In our studies of boundary effects of unconventional superconductors we use the theory of quasiclassical Green's functions introduced by Eilenberger [11]. This approximation of Gorkov's theory is valid in the quasiclassical limit ( $2\pi/k_F \ll \xi$ ). Several review articles have been written on this subject, e.g. by Schmid [12] or Larkin and Ovchinnikov [13]. The quasiclassical propagator in Nambu space

$$\hat{g}(\omega, \mathbf{R}, \mathbf{k}_F) = \begin{pmatrix} g & f \\ f^\dagger & g^\dagger \end{pmatrix} \quad (1)$$

is determined by the Eilenberger equation

$$\left[ \left( \omega + \frac{e}{c} \mathbf{v}_F \cdot \mathbf{A}(\mathbf{R}) \right) \hat{\tau}_3 - \hat{\Delta}(\mathbf{R}, \mathbf{k}_F), \hat{g}(\omega, \mathbf{R}, \mathbf{k}_F) \right] + i\hbar(\mathbf{v}_F \cdot \nabla) \hat{g}(\omega, \mathbf{R}, \mathbf{k}_F) = 0 \quad (2)$$

where  $\hat{\tau}_i$  represent the Pauli matrices and

$$\hat{\Delta}(\mathbf{R}, \mathbf{k}_F) = \begin{pmatrix} 0 & \Delta \\ -\Delta^* & 0 \end{pmatrix}. \quad (3)$$

Additionally a normalization condition is needed to obtain the physical solution of the equation

$$\hat{g}^2(\omega, \mathbf{R}, \mathbf{k}_F) = \hat{1}. \quad (4)$$

The OP must obey the self-consistency equation

$$\hat{\Delta}(\mathbf{R}, \mathbf{k}_F) = - \int_{-\omega_c}^{\omega_c} \frac{d\omega}{4} \langle V(\mathbf{k}_F, \mathbf{k}'_F) \hat{g}^K(\omega, \mathbf{R}, \mathbf{k}'_F) \rangle_{\mathbf{k}'_F}. \quad (5)$$

Here  $\langle \dots \rangle_{\mathbf{k}'_F}$  indicates the average over the Fermi surface. In thermal equilibrium the Keldysh propagator  $\hat{g}^K$  is given by the advanced and retarded propagator  $\hat{g}^{A/R}$

$$\hat{g}^K = (\hat{g}^R - \hat{g}^A) \tanh(\omega/2k_B T) \quad \text{with} \quad \hat{g}^{R/A} : \omega \rightarrow \omega \pm i0_+. \quad (6)$$

For simplicity we make some further assumptions concerning the microscopic properties: For the interaction we choose  $V(\mathbf{k}_F, \mathbf{k}'_F) = V \cos[2(\varphi - \alpha)] \cos[2(\varphi' - \alpha)]$  [25] which generates a  $d$ -wave OP with orientation  $\alpha$  (see Fig. 1)

$$\Delta(\mathbf{R}, \mathbf{k}_F) = \Delta(\mathbf{R}) \cos[2(\varphi - \alpha)]. \quad (7)$$

In addition we assume an isotropic two-dimensional model with a spherical Fermi surface. After the determination of the OP all physical properties can be calculated from the quasiclassical Green's function. For example, the angle-resolved local density of states (DOS) reads

$$\mathcal{N}(\omega, \mathbf{R}, \mathbf{k}_F) = \mathcal{N}_0 \text{Re} [g^R(\omega, \mathbf{R}, \mathbf{k}_F)], \quad (8)$$

where  $\mathcal{N}_0$  is the normal state DOS. In many cases the knowledge of the angle-averaged DOS is sufficient

$$\mathcal{N}(\omega, \mathbf{R}) = \langle \mathcal{N}(\omega, \mathbf{R}, \mathbf{k}_F) \rangle_{\mathbf{k}_F}. \quad (9)$$

The DOS at the surface can directly be measured via the differential conductance  $G = dI/dV$  for normal-metal-insulator-superconductor tunnel-junctions. For  $T \rightarrow 0$  it is given by [18]

$$G(V) = e^2 A \langle v_{F,x} \mathcal{T}(\mathbf{k}_F) \mathcal{N}(eV, x=0, \mathbf{k}_F) \rangle_{(k_{F,x} > 0)}, \quad (10)$$

where the transmission probability is chosen as

$$\mathcal{T}(\varphi) = t^2 \sin^2(\varphi) \ll 1, \quad (11)$$

and  $A$  is the area of the contact. The current-density can be calculated from the Keldysh Green's function via

$$\mathbf{j}(\mathbf{R}) = -e\mathcal{N}_0 \int \frac{d\omega}{4} \langle \mathbf{v}_F \text{Tr}[\hat{\tau}_3 \hat{g}^K(\omega, \mathbf{R}, \mathbf{k}_F)] \rangle_{\mathbf{k}_F}. \quad (12)$$

It has been shown that the decomposition introduced by Maki and Schopohl [26] is suitable for the numerical integration of the Eilenberger equation as well as for analytical considerations (see II B)

$$\hat{g} = \frac{1}{1-ab} \begin{pmatrix} 1+ab & -2a \\ 2b & -(1+ab) \end{pmatrix}. \quad (13)$$

Considering the physical meaning, the functions  $a(\omega, \mathbf{R}, \mathbf{k}_F)$  and  $b(\omega, \mathbf{R}, \mathbf{k}_F)$  are closely related to the particle and hole amplitudes in the Andreev equation as was discussed in detail in [24]. With this construction the normalization condition is obeyed automatically. By

putting in this decomposition in Eq. (2) it can be seen that the functions  $a$  and  $b$  are given by the equations

$$i\hbar(\mathbf{v}_F \cdot \nabla)a = \Delta^* a^2 - 2\omega a + \Delta, \quad (14)$$

$$-i\hbar(\mathbf{v}_F \cdot \nabla)b = \Delta b^2 - 2\omega b + \Delta^*. \quad (15)$$

These equations can be solved on classical trajectories labeled by the Fermi wave vector  $\mathbf{k}_F$ . For each direction  $\mathbf{v}_F$  one has to integrate two ordinary differential equations in order to construct the full propagator.

The Matsubara technique can be used as well to calculate the OP

$$\hat{\Delta}(\mathbf{R}, \mathbf{k}_F) = -k_B T \pi i \sum_{|\omega_n| < \omega_c} \left\langle V(\mathbf{k}_F, \mathbf{k}'_F) \hat{f}^M(\omega_n, \mathbf{R}, \mathbf{k}'_F) \right\rangle_{\mathbf{k}'_F} \quad (16)$$

and the current-density

$$\mathbf{j}(\mathbf{R}) = -e \mathcal{N}_0 k_B T \pi i \sum_{\omega_n} \left\langle \mathbf{v}_F \text{Tr}[\hat{\tau}_3 \hat{g}^M(\omega_n, \mathbf{R}, \mathbf{k}_F)] \right\rangle_{\mathbf{k}_F}. \quad (17)$$

The energy integrals turn to sums over discrete Matsubara frequencies  $\omega_n = k_B T \pi (2n + 1)$  and the Matsubara propagator  $\hat{g}^M$  is determined by the relation

$$\hat{g}^{R/A}(\omega, \mathbf{R}, \mathbf{k}_F) = \hat{g}^M(\omega_n, \mathbf{R}, \mathbf{k}_F) \Big|_{i\omega_n \rightarrow \omega \pm 0_+}. \quad (18)$$

One crucial point for investigating the effects of boundaries is still missing. As the quasiclassical condition does not apply in the vicinity of surfaces and interfaces we have to treat the scattering of quasiparticles by effective boundary conditions. The properties of the boundary enter the calculations only at this point.

## B. Boundary Conditions

In our work we use the general theory recently derived in [24]. The starting point is the Andreev-like equation for the particle- and hole-like amplitudes which factorize the Eilenberger Green's function in Eq. 1 (see [24] for details). In this approach, it is possible to consider roughness that occurs on length scales much smaller than the coherence length. All information on the microscopic shape of the boundary is provided by the scattering amplitudes from the in-trajectories ( $k_{F,x}^{\text{in}} < 0$ ) to the out-trajectories ( $k_{F,x}^{\text{out}} > 0$ ); they are gathered in the scattering matrix  $\mathbf{S}$ .

For simplicity we consider only a finite number  $n$  of discrete in- and out-trajectories  $\mathbf{k}_F^{\text{in/out}} \rightarrow \mathbf{k}_{F,i}^{\text{in/out}}$ ,  $i = 1, 2, \dots, n$  with equidistant angles. Following [24] the boundary conditions are determined using the functions

$$A_l(\beta) = \det[\mathbf{1} - \mathbf{S} \hat{a} \mathbf{S}^\dagger \hat{b}_l^\beta], \quad (19)$$

$$B_l(\alpha) = \det[\mathbf{1} - \mathbf{S} \hat{a}_l^\alpha \mathbf{S}^\dagger \hat{b}], \quad (20)$$

with the diagonal  $n \times n$ -matrices

$$\begin{aligned}\hat{a} &= \text{diag}\{a_1, \dots, a_n\}, & \hat{a}_l^\alpha &= \text{diag}\{a_1, \dots, a_{l-1}, \alpha, a_{l+1}, \dots\}, \\ \hat{b} &= \text{diag}\{b_1, \dots, b_n\}, & \hat{b}_l^\beta &= \text{diag}\{b_1, \dots, b_{l-1}, \beta, b_{l+1}, \dots\}, \\ \text{and} & & a_i &= a(\omega, x = 0, \mathbf{k}_{\text{F},i}^{\text{in}}), & b_i &= b(\omega, x = 0, \mathbf{k}_{\text{F},i}^{\text{out}}).\end{aligned}\tag{21}$$

The solutions of  $A_l(\beta) = 0$  and  $B_l(\alpha) = 0$  provide the boundary conditions

$$A_l(\beta_0) = 0 \quad \Rightarrow \quad a(\omega, x = 0, \mathbf{k}_{\text{F},l}^{\text{out}}) = \frac{1}{\beta_0},\tag{22}$$

$$B_l(\alpha_0) = 0 \quad \Rightarrow \quad b(\omega, x = 0, \mathbf{k}_{\text{F},l}^{\text{in}}) = \frac{1}{\alpha_0}.\tag{23}$$

As the determinant is a linear function of each of the matrix elements the functions  $A_l(\beta)$  and  $B_l(\alpha)$  are linear in  $\beta$  and  $\alpha$ . We can solve the boundary condition by calculating  $A_l(\beta)$  and  $B_l(\alpha)$  for two arbitrary values of  $\beta$  and  $\alpha$ ; for  $\beta = 0, 1$  and  $\alpha = 0, 1$  we obtain

$$a(\omega, x = 0, \mathbf{k}_{\text{F},l}^{\text{out}}) = 1 - \frac{A_l(1)}{A_l(0)},\tag{24}$$

$$b(\omega, x = 0, \mathbf{k}_{\text{F},l}^{\text{in}}) = 1 - \frac{B_l(1)}{B_l(0)}.\tag{25}$$

With the boundary condition the Green's function can be calculated: At first the integration of Eq. (14) on the in- and of Eq. (15) on the out-trajectories is performed starting from the known bulk values [24]

$$a(\omega, x \rightarrow \infty, \mathbf{k}_{\text{F}}^{\text{in}}) = \frac{\Delta_\infty(\mathbf{k}_{\text{F}}^{\text{in}})}{\omega + \sqrt{\omega^2 - |\Delta_\infty(\mathbf{k}_{\text{F}}^{\text{in}})|^2}},\tag{26}$$

$$b(\omega, x \rightarrow \infty, \mathbf{k}_{\text{F}}^{\text{out}}) = \frac{\Delta_\infty^*(\mathbf{k}_{\text{F}}^{\text{out}})}{\omega + \sqrt{\omega^2 - |\Delta_\infty(\mathbf{k}_{\text{F}}^{\text{out}})|^2}}\tag{27}$$

towards the boundary ( $\Delta_\infty$ : bulk OP). Then the boundary conditions must be applied to get the  $a$ 's on the out- and the  $b$ 's on the in-trajectories at the boundary and the succeeding integration on these trajectories provides the missing  $a$ 's and  $b$ 's.

The properties of the boundaries enter only via the  $S$ -matrix. The value  $|S_{ij}|^2$  is the probability of scattering from  $\mathbf{k}_{\text{F},j}^{\text{in}}$  to  $\mathbf{k}_{\text{F},i}^{\text{out}}$ . We choose the numbering of the trajectories so that  $\mathbf{S} = \mathbf{1}$  reproduces the specular case. Due to current conservation  $\mathbf{S}$  must be unitary

$$\mathbf{S}\mathbf{S}^\dagger = \mathbf{1}.\tag{28}$$

With a suitable choice of  $\mathbf{S}$  arbitrary physical situations can be treated by this technique. Some examples are presented in chapter III.

We are also able to connect basic symmetries of the physical situation with transformation properties of the scattering matrix. The symmetry operations for the mirror and the time-reversal symmetry are illustrated in Fig. 3. The mirror symmetry of the surface ( $y \rightarrow -y$ ) is given by the transformation

$$\mathbf{S}' = \mathbf{T}\mathbf{S}\mathbf{T}, \quad \text{with} \quad T_{ij} = \delta_{(n+1-i),j}.\tag{29}$$

The time-reversal symmetry operation is represented by

$$\mathbf{S}' = \mathbf{T}\mathbf{S}^T\mathbf{T}.\tag{30}$$

### III. RESULTS FOR DIFFERENT SURFACES

Since we are discussing different types of roughness which occur in experiments we have to find adequate scattering matrices for each situation. As the unitarity condition (28) must be obeyed we represent  $\mathbf{S}$  by the relation

$$\mathbf{S} = \exp\{i\mathbf{H}\} \quad \text{with} \quad \mathbf{H} = \mathbf{H}^\dagger. \quad (31)$$

In the subsequent sections III A and III B we present S-matrices for random surfaces as well as for surfaces with small tilted mirrors and physical properties such as the OP and the DOS in the vicinity of a surface. The retarded Green's-function should be evaluated at  $\omega \rightarrow \omega + i\delta$ ; for numerical purposes we keep  $\delta$  finite. For the calculation of the DOS we choose  $\delta = 0.02k_{\text{B}}T_c$  and  $n = 200$ ; we checked that the results do not change for larger  $n$ .

#### A. Random surface

In this section we search for a scattering matrix that can describe random surfaces. To take into account the statistical properties of the surfaces we choose a random matrix in this approach; therefore the Hermitian matrix  $\mathbf{H}$  is assumed to be a member of the Gaussian unitary ensemble (GUE) as was also suggested by Yamada *et al.* [22]

$$\begin{aligned} \langle H_{ij} \rangle &= 0, \\ \langle H_{ij}^* H_{i'j'} \rangle &= \frac{\tau}{n} \delta_{ii'} \delta_{jj'}. \end{aligned} \quad (32)$$

The brackets  $\langle \dots \rangle$  denote the ensemble average of the disorder. The roughness of the surface can be varied by the parameter  $\tau$ . The factor  $1/n$  in the correlator of  $\mathbf{H}$  ensures that the whole procedure does not depend on the number of channels for  $n \rightarrow \infty$ .

The averaged scattering probabilities  $\langle |S_{ij}|^2 \rangle$  have a simple behavior. For  $\tau = 0$  only  $|S_{ii}|^2 = 1$  are finite and all other elements are zero. If  $\tau$  is increased the diagonal elements (responsible for specular reflection) are reduced to  $\langle |S_{ii}|^2 \rangle = |u(\tau)|^2 < 1$  and the off-diagonal elements become finite  $\langle |S_{i \neq j}|^2 \rangle = |v(\tau)|^2 \lesssim 1/n$  (see Fig. 4) with

$$|u(\tau)|^2 + (n-1)|v(\tau)|^2 = 1. \quad (33)$$

Therefore, the averaged properties of  $\mathbf{S}$  are fully determined by the probability for specular reflection  $|u|^2$  and we can use it as a measure for the disorder of the surface; its relation to the parameter  $\tau$  is shown in Fig. 5. For  $\tau$  small enough, the reflection is partially specular. When  $\tau \gtrsim 2$ , the scattering becomes isotropic since  $|u|^2 \sim |v|^2 \sim 1/n$ . We call this situation the diffusive limit.

We apply a random matrix  $\mathbf{S}$  to calculate the OP and the DOS in the vicinity of a disordered surface. We study several (up to 50) realizations of the S-matrix individually. We find that the fluctuations are small as can be seen in Fig. 6. Therefore, it is meaningful to consider the averaged quantities  $\langle \Delta \rangle$  and  $\langle G \rangle$ . The results for  $\alpha = 0^\circ, 45^\circ$  and different roughness values are shown in figs. 7 and 8 for the OP and for the differential conductance in figs. 9 and 10, where the normal state resistance is used

$$R_N^{-1} = e^2 A \mathcal{N}_0 t^2 v_F \frac{4}{3\pi}. \quad (34)$$

Additionally the angle-dependent DOS is presented in Fig. 11 for the medium roughness  $\tau = 0.4$ .

We point out some interesting features of the model: Disorder leads to a suppression and broadening of the ZBCP for  $\alpha = 45^\circ$ . By comparison with experimental data [10] realistic results can be achieved by  $0.8 \lesssim \tau \lesssim 2$ . In our model with disorder, for  $\alpha = 0^\circ$  no ZBCP occurs. In the angle-resolved DOS no splitting of any bound states due to disorder is seen. In the diffusive limit the OP reaches an almost universal curve independent of the surface orientation  $\alpha$ ; the conductance becomes flat and is of the order of the normal state value for all energies and surface orientations.

## B. Surface with small tilted mirrors

With this method also other roughness types can be studied. In this section we consider surfaces which only connect few trajectories. For example one can think of small (compared to the coherence length) mirrors with distinct orientations. Each of the mirrors contributes to reflection so that the surface acts as a beam-splitter. For the mirror orientations  $\theta = 180^\circ l/m$  with integer  $l = -m + 1, \dots, m - 1$ , this can be achieved by the choice

$$\mathbf{H} = \tau \tilde{\mathbf{H}} \quad \text{with} \quad \tilde{H}_{ij} = \sum_{l=1}^{m-1} \delta_{|i-j|, ln/m}. \quad (35)$$

In the further calculation we choose  $n$  to be a multiple of  $m$ ; this leads to a simpler form of  $\mathbf{S}$  but has no physical implication for  $n \gg m$ . In this case  $\tilde{\mathbf{H}}$  considered as a block  $m \times m$  matrix has zeros on the diagonal, and all other elements are equal to  $\mathbf{1}_{n/m}$  ( $(n/m) \times (n/m)$  unity matrix). Since

$$\tilde{\mathbf{H}}^2 = (m - 1)\mathbf{1} + (m - 2)\tilde{\mathbf{H}} \quad (36)$$

the exponential representation for the  $S$ -matrix in Eq. (31) becomes

$$\mathbf{S} = u(\tau)\mathbf{1} + v(\tau)\tilde{\mathbf{H}}, \quad (37)$$

where

$$|u|^2 + (m - 1)|v|^2 = 1, \quad (38)$$

$$uv^* + u^*v + (m - 2)|v|^2 = 0 \quad (39)$$

as required by the unitarity of the  $S$ -matrix. For fixed  $\tau$  the value of  $|u|^2$  is the probability for specular reflection, whereas  $|v|^2$  is the probability for the scattering on one of the tilted mirrors. The scattering matrix can be calculated explicitly and the amplitudes are given by

$$u(\tau) = \frac{e^{-i\tau}}{m}(m - 1 + e^{im\tau}), \quad (40)$$

$$v(\tau) = \frac{e^{-i\tau}}{m}(e^{im\tau} - 1). \quad (41)$$



Therefore the probability for specular reflection (mirror with  $\theta = 0$ ) is given by

$$|u(\tau)|^2 = \frac{1}{m^2}[(m-1)^2 + 1 + 2(m-1)\cos(m\tau)]. \quad (42)$$

In this model, each incoming trajectory is split into  $m$  outgoing trajectories. Altogether, there are  $m$  in-trajectories which are scattered into the same out-states. In the terminology of [24], this corresponds to a *knot* with  $m$  in- and  $m$  out-trajectories (see Fig. 12).

We study the simplest case  $m = 2$  with three mirrors with orientation  $\theta = 0^\circ, \pm 45^\circ$ , where two in- and two out-trajectories are coupled. The  $S$ -matrix has the form

$$\mathbf{S} = \begin{pmatrix} \mathbf{u} & \mathbf{v} \\ \mathbf{v} & \mathbf{u} \end{pmatrix} \quad (43)$$

with  $\mathbf{u} = u\mathbf{1}_{n/2}$  and  $\mathbf{v} = v\mathbf{1}_{n/2}$ ; the functions  $u$  and  $v$  are given by

$$u(\tau) = \cos(\tau), \quad v(\tau) = i \sin(\tau). \quad (44)$$

For  $\alpha = 0^\circ$  and  $|u|^2 < 1$  finite energy bound states occur; their energies move to zero with decreasing weight of specular reflection. If  $|u|^2 = 0$  ( $\tau = \pi/2$ ), i.e. no specular reflection is present, the bound states reach zero energy. For  $\alpha = 45^\circ$  this is reversed: non-specular reflection leads to a splitting of the zero energy bound states, which grows with decreasing  $|u|^2$  (Fig. 13), as was discussed qualitatively in [24]. This model is in some aspects similar to a Josephson-contact with a specular interface, where also a splitting of the zero energy bound state can be observed.

The case  $m > 2$ , however, is more complex and cannot be mapped to any studied model. We consider the case  $m = 3$ . The five mirrors have the relative orientations  $\theta = 0^\circ, \pm 30^\circ, \pm 60^\circ$  and three in- and three out-trajectories are connected; the  $S$ -matrix is given by

$$\mathbf{S} = \begin{pmatrix} \mathbf{u} & \mathbf{v} & \mathbf{v} \\ \mathbf{v} & \mathbf{u} & \mathbf{v} \\ \mathbf{v} & \mathbf{v} & \mathbf{u} \end{pmatrix} \quad (45)$$

with  $\mathbf{u} = u\mathbf{1}_{n/3}$  and  $\mathbf{v} = v\mathbf{1}_{n/3}$ . As can be seen in Eq. (42) for  $m = 3$  it is only possible to choose the specular scattering probability in the interval  $|u|^2 \in [1/9, 1]$ . For  $\alpha = 0^\circ$  non-specular scattering leads to finite energy bound states which are moving to lower energies with decreasing  $|u|^2$ ; but here zero energy is not reached. In the case of  $\alpha = 45^\circ$  for  $|u|^2 < 1$  one part of the zero energy bound state splits to finite energies, whereas another part stays at zero energy with reduced spectral weight (Fig. 14). In figs. 15 we also present the case  $m = 4$  with 7 different mirrors for the surface orientations  $\alpha = 0^\circ, 45^\circ$ .

Summing up our observations for the  $\alpha = 45^\circ$  case small mirrors reduce the spectral weight of the zero energy bound states as a part splits to finite energies. For the surface orientation  $\alpha = 0^\circ$  in general (except some particular situations) no zero energy bound state is produced.

Finally we point out that a larger class of  $S$ -matrices can be used to describe such surfaces

$$H_{ij} = \sum_{l=1}^{m-1} \tau_l \delta_{|i-j|, ln/m}. \quad (46)$$

This model has almost the same properties as (35), however, the scattering probabilities for each mirror differ. Moreover it is possible to combine these mirrors with disorder just by multiplying the related  $S$ -matrices and averaging as in section III A.

#### IV. DISCUSSION AND CONCLUSION

In the present paper, the scattering matrix approach has been applied to describe  $d$ -wave superconductors in the vicinity of rough surfaces. Two physical situations are examined: (i) a surface with partially diffusive reflection described by random scattering matrices; (ii) a surface with small tilted mirrors (facets) where the reflected wave is a coherent mixture of waves propagating in several directions.

First, for the diffusive surface it appears that our results are very similar to those found in other approaches such as the randomly rippled wall model [22] or the thin dirty layer [18]. In contrast to those calculations we treated the disorder by direct sampling. We find that the deviation of the DOS from the average is rather small. Therefore, our calculations confirm the validity of averaging procedures used in the afore-mentioned papers. In particular the broadening of the ZBCP due to increasing disorder is no artifact of the approximate averaging. (Other models exist that show no such broadening [20,27].)

Second, we studied a surface with tilted mirrors. In contrast to the model for large facets examined in [15], our model describes a surface where faceting occurs on a scale small compared to the coherence length. These two models provide qualitatively different results: our model in general shows no ZBCP for  $\alpha = 0$ , whereas large facets lead to a ZBCP for each surface orientation.

In experiments on high- $T_c$  materials, it cannot be excluded that roughness on a scale of the coherence length or larger occurs, which is beyond the model used in the current paper. This might be the case in the experiment described in [10], where the width of the ZBCP is constant with varying disorder. In some experiments [8,9] a ZBCP for  $\alpha = 0$  is observed, too, consistent with the model for large facets [15].

#### ACKNOWLEDGMENTS

We would like to thank Y. Barash, M. Dzierzawa, M. Fogelström, and J. Mannhart for helpful discussions. This work was supported in part by the DAAD, the BMBF (project number 13N6918/1), and the Swedish Institute.

## REFERENCES

- [1] C.C. Tsuei, J.R. Kirtley, C.C. Chi, Lock See Yu-Jahnes, A. Gupta, T. Shaw, J.Z. Sun, and M.B. Ketchen, Phys. Rev. Lett. **73**, 593 (1994).
- [2] J. Geerk, X.X. Xi, and G. Linker, Z. Phys. B **73**, 329 (1988).
- [3] D. Mandrus, L. Forro, D. Koller, and L. Mihaly, Nature (London) **351**, 460 (1991).
- [4] J. Lesueur, L.H. Greene, W.L. Feldman, and A. Inam, Physica C **191**, 325 (1992).
- [5] S. Kashiwaya, Y. Tanaka, M. Koyanagi, H Takashima, and K. Kajimura, Phys. Rev. B **51**, 1350 (1995).
- [6] L. Alff, H. Takashima, S. Kashiwaya, N. Terada, H. Ihara, Y. Tanaka, M. Koyanagi, and K. Kajimura, Phys. Rev. B **55**, R14757 (1997).
- [7] C.-R. Hu, Phys. Rev. Lett. **72**, 1526 (1994).
- [8] M. Covington, M. Aprili, E. Paraoanu, and L.H. Greene, Phys. Rev. Lett. **79**, 277 (1997).
- [9] J.Y.T. Wei, N.-C. Yeh, D.F. Garrigus, and M. Strasik, Phys. Rev. Lett. **81**, 2542 (1998).
- [10] M. Aprili, M. Covington, E. Paraoanu, B. Niedermeier, and L.H. Greene, Phys. Rev. B **57**, R8139 (1998).
- [11] G. Eilenberger, Z. Phys. **214**, 195 (1968).
- [12] A. Schmid, in: *Nonequilibrium Superconductivity*, edited by K.E. Gray (Plenum, N.Y., 1981).
- [13] A.I. Larkin and Yu.N. Ovchinnikov, in: *Nonequilibrium Superconductivity*, edited by D.N. Langenberg and A.I. Larkin (Elsevier, Amsterdam, 1984).
- [14] M. Matsumoto and H. Shiba, J. Phys. Soc. Jpn. **64** 3384 (1995); **64** 4867 (1995).
- [15] M. Fogelström, D. Rainer, and J.A. Sauls, Phys. Rev. Lett. **79** 281 (1997).
- [16] A. V. Zaitsev, Sov. Phys. JETP **59**, 1015 (1984).
- [17] Yu.N. Ovchinnikov, Sov. Phys. JETP **29**, 853 (1969).
- [18] Yu.S. Barash, A.A. Svidzinsky, and H. Burkhardt, Phys. Rev. B **55** 15282 (1997).
- [19] A. Poenicke, M. Fogelström, and J.A. Sauls, Physica B, to be published (2000).
- [20] A. Poenicke, Yu.S. Barash, C. Bruder, and V. Istyukov, Phys. Rev. B **59** 7102 (1999).
- [21] Y. Nagato, S. Higashitani, K. Yamada, and K. Nagai, J. Low Temp. Phys. **103**, 1 (1996).
- [22] K. Yamada, Y. Nagato, S. Higashitani, and K. Nagai, J. Phys. Soc. Jpn. **65**, 1540 (1996).
- [23] J. Mannhart et al., Phys. Rev. Lett. **77**, 2782 (1996).
- [24] A. Shelankov and M. Ozana, Phys. Rev. B **61**, 7077 (2000).
- [25] L.J. Buchholtz, M. Palumbo, D. Rainer, and J.A. Sauls, J. Low Temp. Phys. **101**, 1079 (1995); **101**, 1099 (1995).
- [26] N. Schopohl and K. Maki, Phys. Rev. B **52**, 490 (1995).
- [27] M.B. Walker and P. Pairor, Phys. Rev B **60**, 10395 (1999).

FIGURES

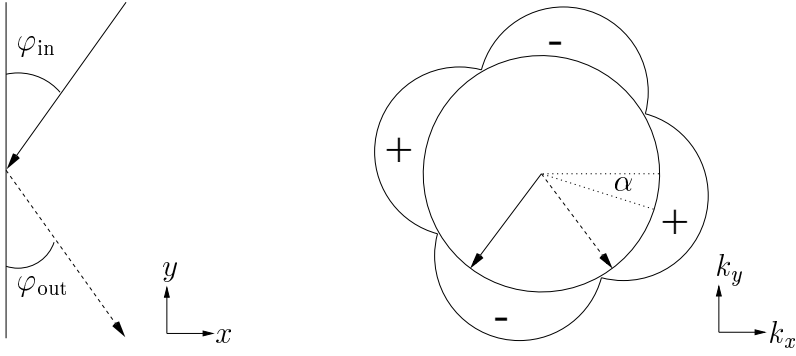


FIG. 1. Surface effect in real space (left) and  $k$ -space (right).

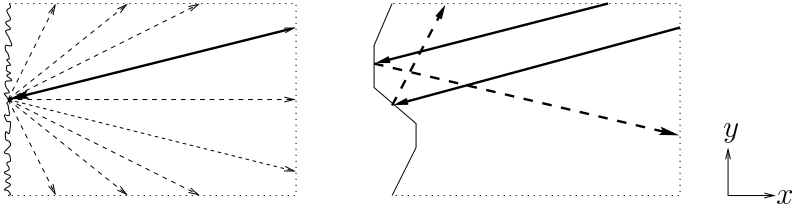


FIG. 2. Effect of roughness on small (left) and large (right).

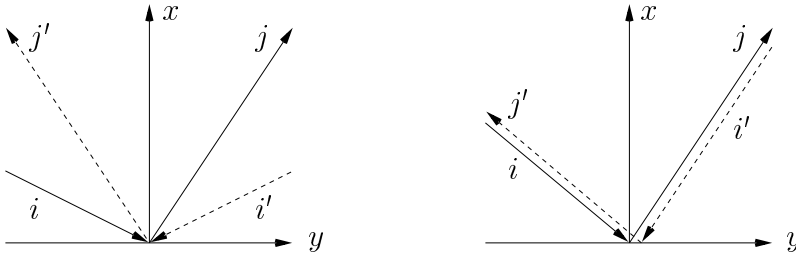


FIG. 3. Two trajectories (solid and dashed line) are plotted which are connected via symmetry transformation for mirror (left) and time-reversal symmetry (right).

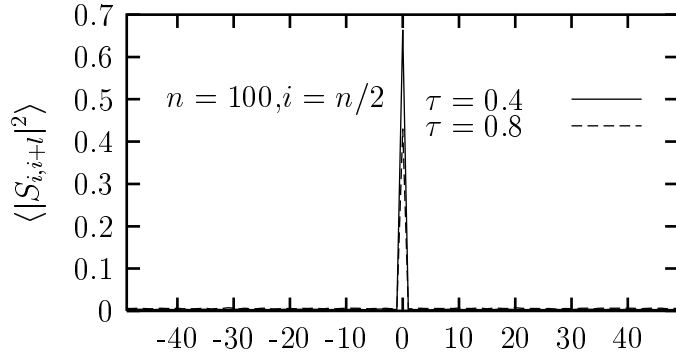


FIG. 4. Mean scattering probability from the in-trajectories ( $i + l$ ) to a fixed out-trajectory  $i = n/2$  for different values of  $\tau$ . The specular contribution is reduced by increasing  $\tau$ .

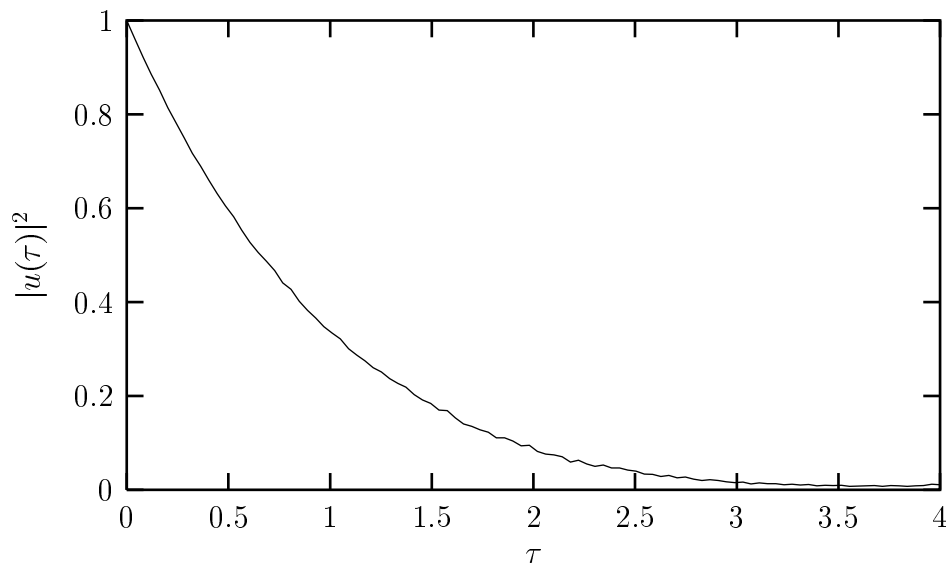


FIG. 5. Specular scattering weight as a function of  $\tau$ . The diffusive limit is reached for  $\tau \gtrsim 2$ .

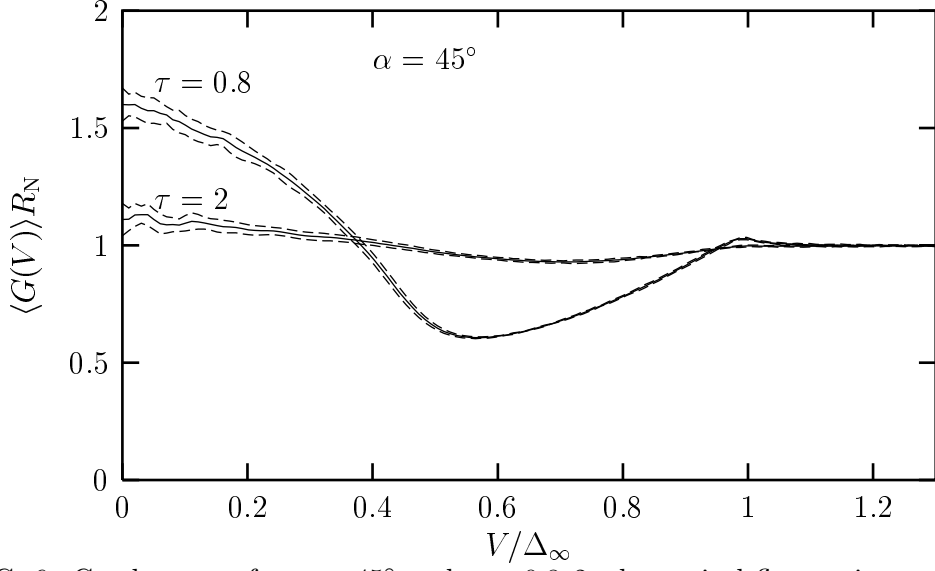


FIG. 6. Conductance for  $\alpha = 45^\circ$  and  $\tau = 0.8, 2$ ; the typical fluctuations are confined by the dashed lines.

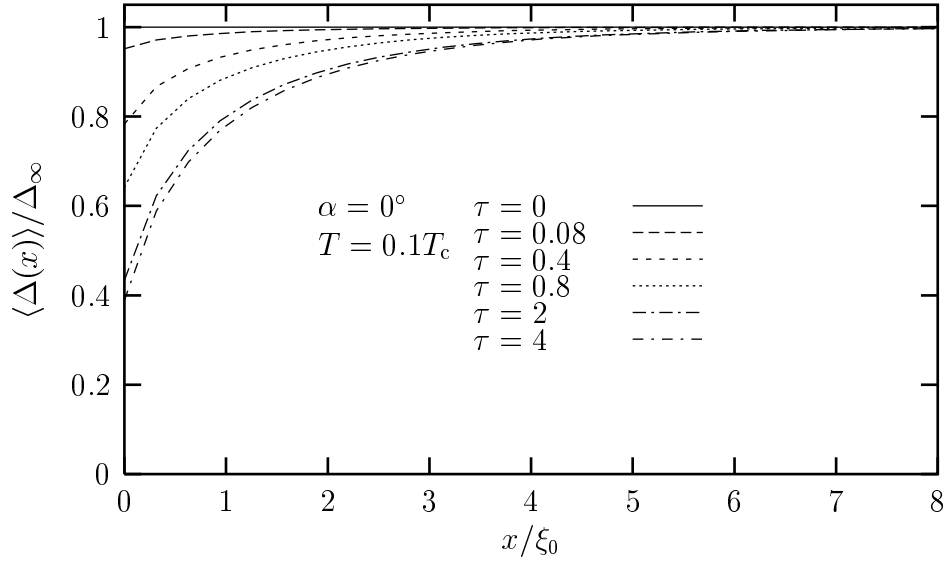


FIG. 7. Averaged order parameter for  $\alpha = 0^\circ$  and  $\tau = 0, 0.08, 0.4, 0.8, 2, 4$ .

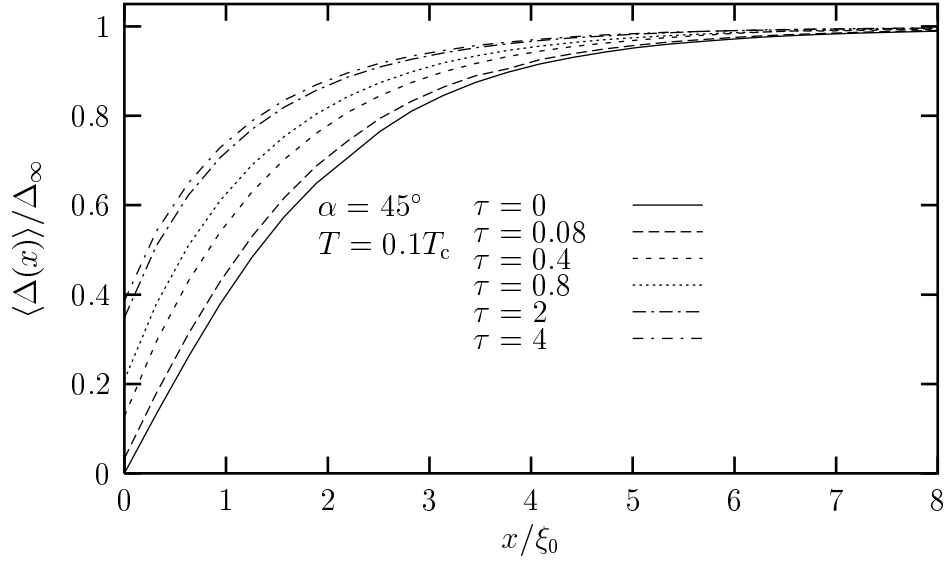


FIG. 8. Averaged order parameter for  $\alpha = 45^\circ$  and  $\tau = 0, 0.08, 0.4, 0.8, 2, 4$ .

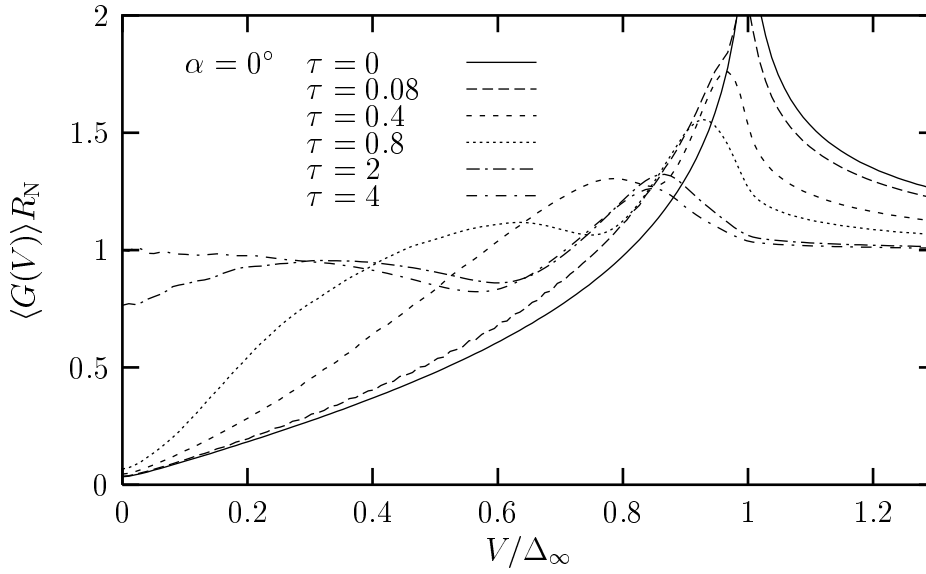


FIG. 9. Averaged differential conductance for  $\alpha = 0^\circ$  and  $\tau = 0, 0.08, 0.4, 0.8, 2, 4$ .

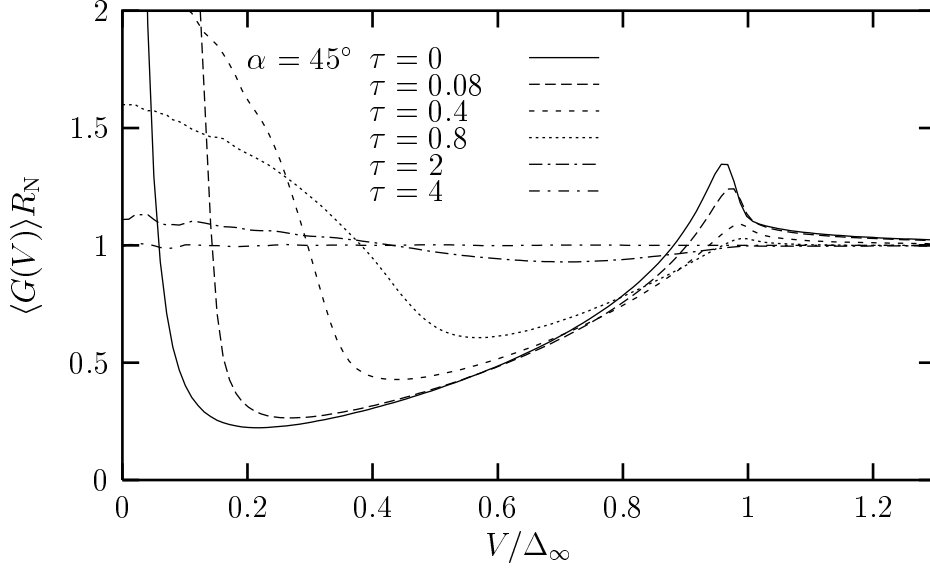


FIG. 10. Averaged differential conductance for  $\alpha = 45^\circ$  and  $\tau = 0, 0.08, 0.4, 0.8, 2, 4$ .

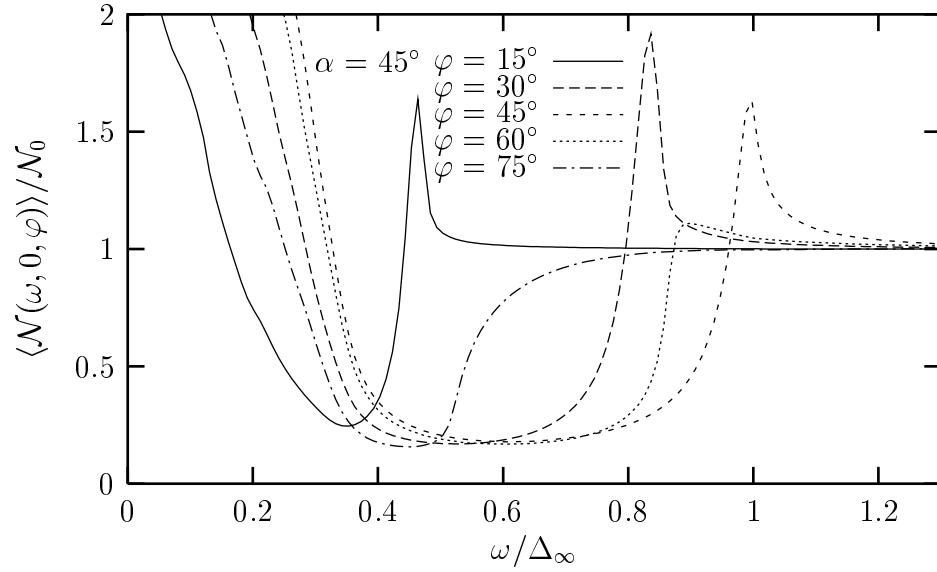


FIG. 11. Averaged angle-resolved DOS for  $\alpha = 45^\circ$  and  $\tau = 0.4$ .

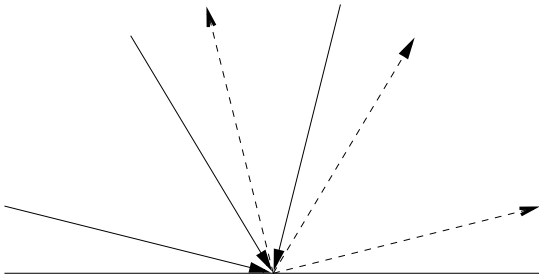


FIG. 12. For  $m = 3$  each of the three in-trajectories (solid lines) contributes to the same three out-trajectories (dashed lines).



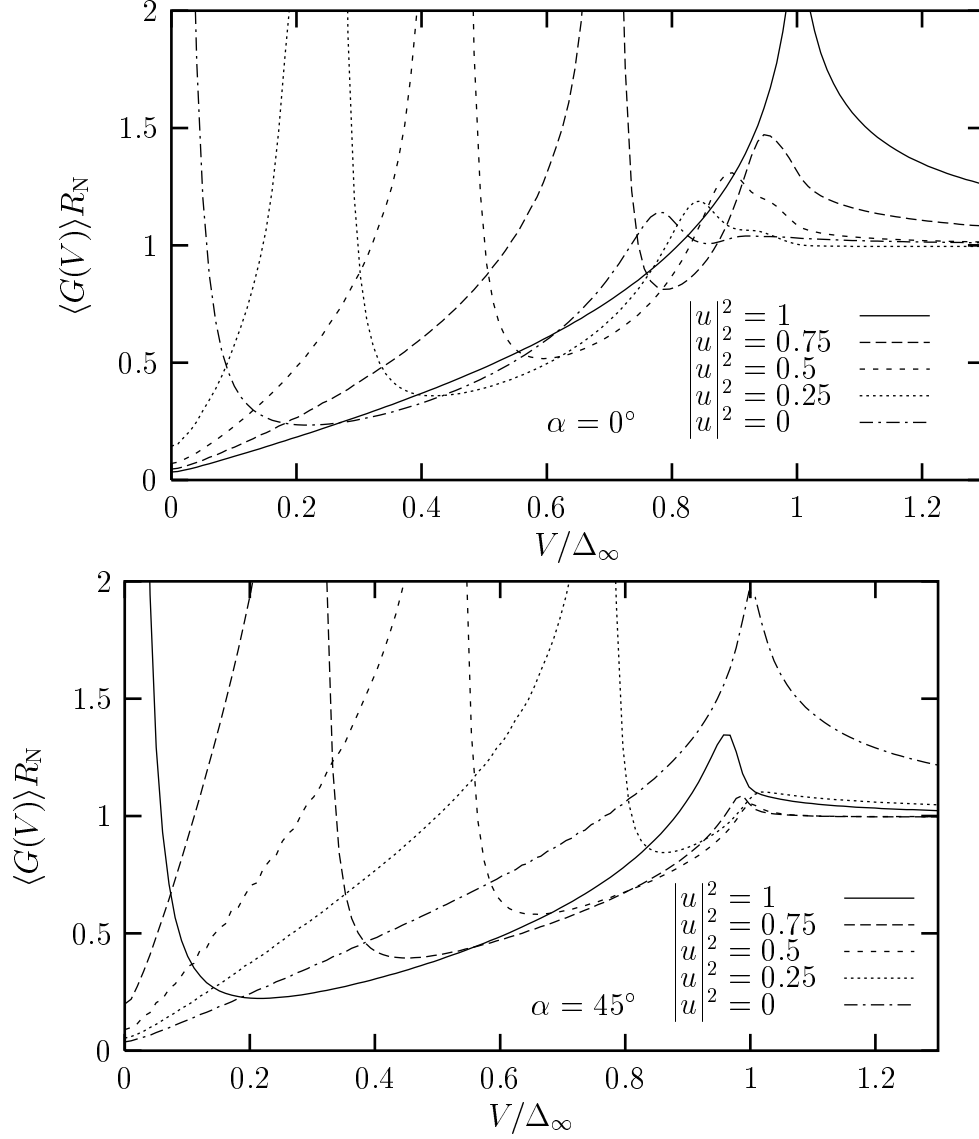


FIG. 13. Differential conductance for  $m = 2$  and  $\alpha = 0^\circ, 45^\circ$ ; the specular scattering weight is varied.

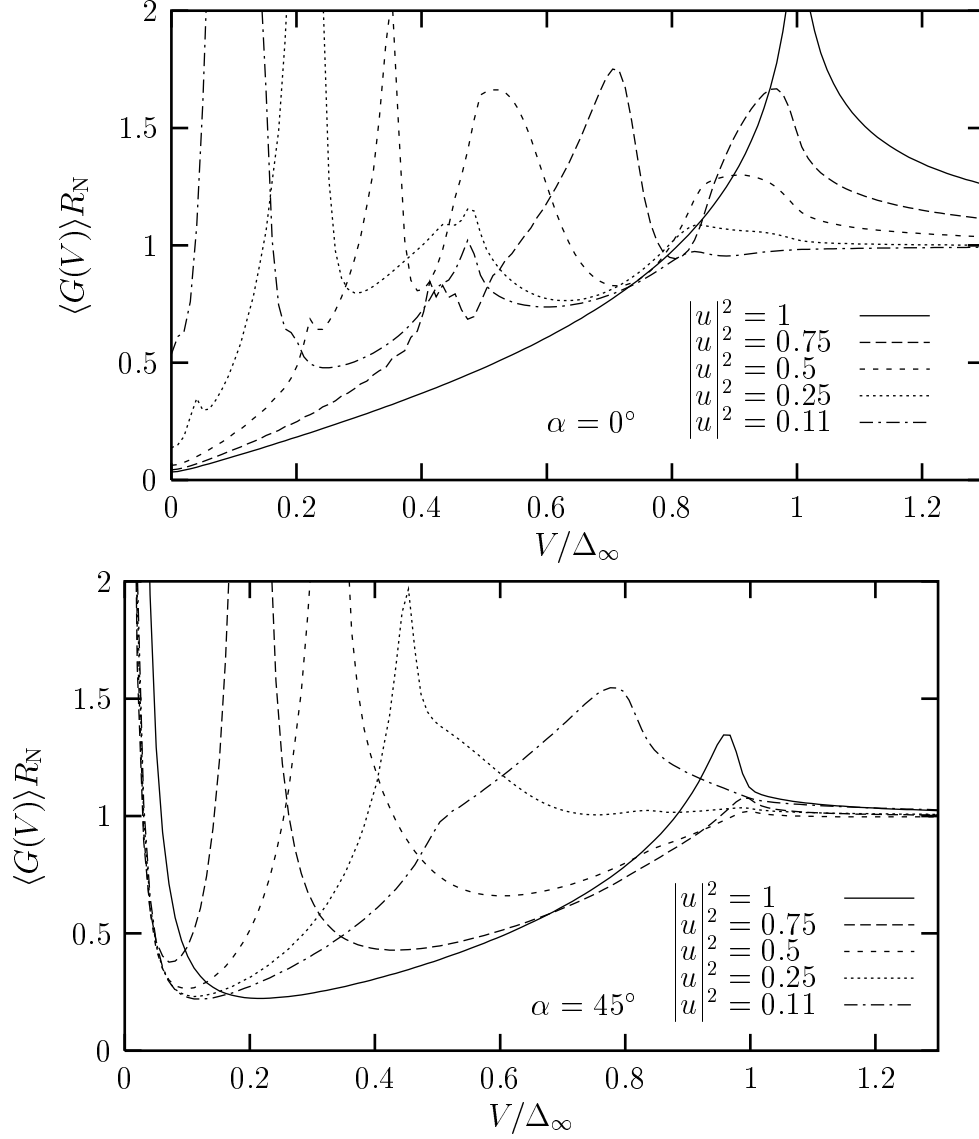


FIG. 14. Differential conductance for  $m = 3$  and  $\alpha = 0^\circ, 45^\circ$ ; the specular scattering weight is varied.

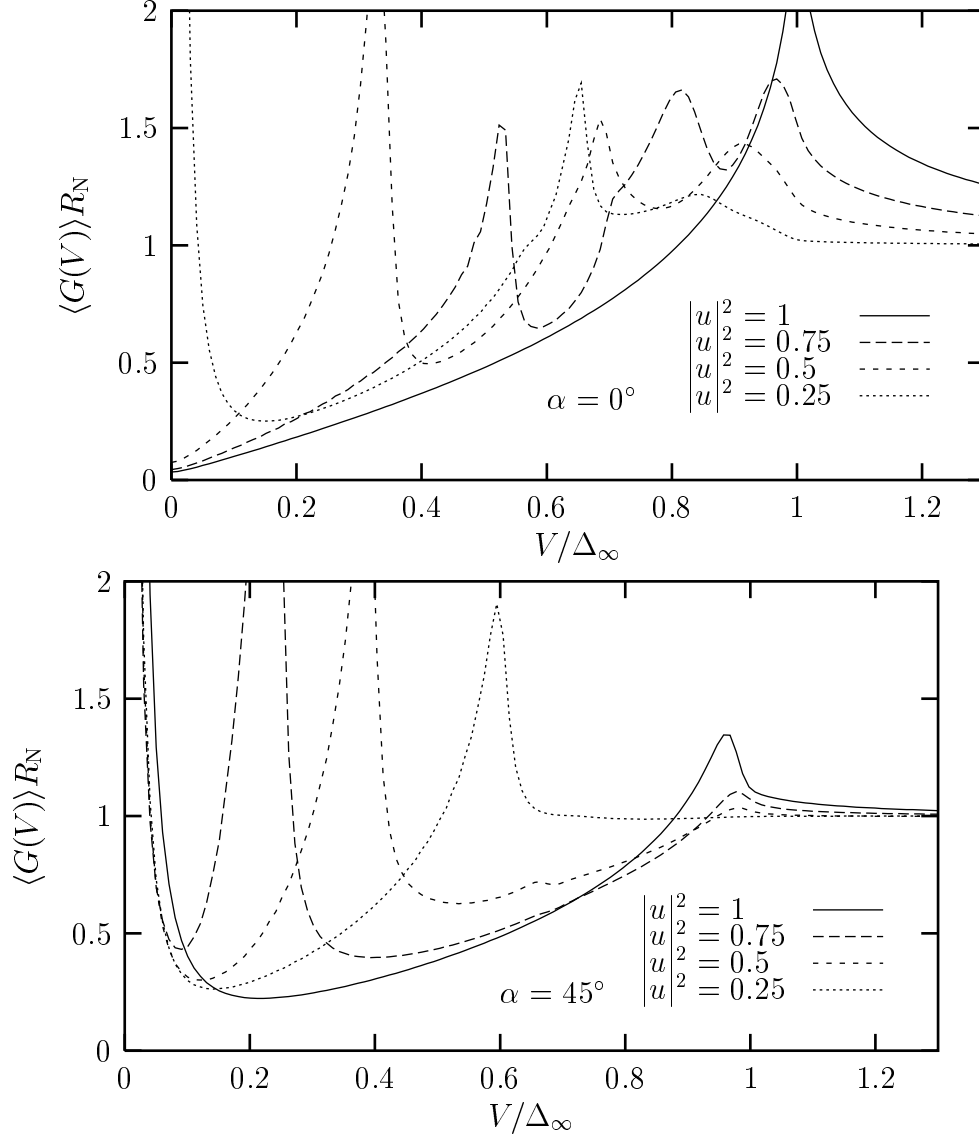


FIG. 15. Differential conductance for  $m = 4$  and  $\alpha = 0^\circ, 45^\circ$ ; the specular scattering weight is varied.